Research Article | Vol. 3, No. 6 / 15 June 2020 / OSA Continuum 1536

High efficiency cascaded third-harmonic generation in a quasi-periodically poled $KTiOPO_4$ crystal

AUGUSTIN VERNAY,[1] LUCAS BONNET-GAMARD,[1] VÉRONIQUE BOUTOU,[1] SIVAN TRAJTENBERG-MILLS,[2] ADY ARIE,[2] AND BENOÎT BOULANGER[1,*]

[1] *Univ. Grenoble Alpes, CNRS, Grenoble INP, Institut Néel, 38000 Grenoble, France*
[2] *US School of Electrical Engineering, Faculty of Engineering, Tel Aviv University, Tel Aviv, Israel*
[*] *benoit.boulanger@neel.cnrs.fr*

Abstract: We performed and studied cascaded third-harmonic generation (THG) in a quasi-periodically poled KTP (QPPKTP) crystal allowing simultaneous phase-matching of the two cascading steps $\omega + \omega \rightarrow 2\omega$ and $2\omega + \omega \rightarrow 3\omega$. The phase-matching was achieved at the fundamental wavelength $\lambda_\omega = 1587$ nm when the QPPKTP crystal was heated to 95°C. The energy conversion efficiency reached 40% in the picosecond regime for a fundamental energy of 20 μJ that corresponds to an intensity of 1.5 GW/cm^2. It is the highest value of THG efficiency ever reported to the best of our knowledge. The modeling in the case of the depleted pump regime accurately described the experiments.

1. Introduction

Extending the bandwidth of laser sources is a huge field of application of parametric nonlinear optics starting from the pioneering work on second-harmonic generation (SHG) [1] and optical parametric oscillators (OPO) [2]. Third-harmonic generation (THG) is also of strong interest in this frame of frequency conversion since it is often used as a pump source of OPO [3], but it is also at the heart of nuclear reactions [4] and optical processing [5] for example. Quantum optics is another area of interest for THG since it can lead to the generation of squeezed light [6,7].

THG can be performed using a direct third order nonlinear process, *i.e.* $\omega + \omega + \omega \rightarrow 3\omega$ that is governed by the third-order nonlinear electric susceptibility $\chi^{(3)}$ [8]. While third-order susceptibility is present in all materials, it is usually very small, causing conversion efficiency of THG to be low and requires very high pump intensities. Another approach is by cascading two processes driven by the second-order susceptibility $\chi^{(2)}$: $\omega + \omega \rightarrow 2\omega$, which corresponds to SHG, and THG it-self, *i.e.* $2\omega + \omega \rightarrow 3\omega$ creating the third harmonic. These two steps can be successive [4] or simultaneous [7,9,10,11].

The second-order susceptibility is available only for non-centrosymmetric materials, but it can be a few orders of magnitude higher than the third-order susceptibility, so that the second-order processes are generally more efficient. Direct as well as cascaded THG can be achieved in phase-matched birefringent crystals of volume [8,10,12] or waveguide [11,13] dimensions. But periodically-poled nonlinear crystals are also a good alternative because of their relatively high non-linearity and their phase-matching flexibility [6,7,14]. Note that the simultaneous cascading configuration had led to the highest THG conversion efficiencies using birefringent phase-matching [10] as well as quasi-phase-matching [9,11].

The present study deals with this latter configuration. We developed theoretical and experimental methods for designing an efficient cascaded THG using a single quasi-periodically poled $KTiOPO_4$ crystal (QPPKTP). KTP crystals are widely used for frequency conversion and quantum optics, they have a high second-order susceptibility and are commercially available. Quasi

#395084 https://doi.org/10.1364/OSAC.395084
Journal © 2020 Received 13 Apr 2020; accepted 19 May 2020; published 1 Jun 2020

OSA CONTINUUM

periodic structures in KTP have shown to be strong contenders for achieving high conversion efficiencies [9,15,16]. Our objective is then to go beyond these pioneering works by developing a model of THG in the depleted pump regime and by experimentally optimizing the conversion efficiency, in particular in the visible around 0.5 µm. This last point is of prime importance in the more general framework of the generation of new quantum states of light, where the exact reverse of cascaded THG, *i.e.* $3\omega \rightarrow \omega + 2\omega$ coupled with $2\omega \rightarrow \omega + \omega$, is a way to produce three highly correlated photons at ω [17]. The target is then to perform this triple-photon generation (TPG) in the telecom range for quantum information, which means λ_ω around 1.5 µm and so $\lambda_{3\omega}$ around 0.5 µm. Since TPG and THG exhibit the same phase-matching properties, the optimization of one then leads to the optimization of the other.

2. Crystal design

Tailoring the second-order susceptibility of nonlinear crystals can be performed by electric field poling, a process that can flip the sign of some $\chi^{(2)}$ coefficients. The most common use of this is for quasi-phase matching, where a periodic change in the sign of the susceptibility with period Λ can compensate phase mismatch, leading to high conversion efficiencies in crystals and processes that were inefficient otherwise. But not only periodic structures can be created, also 2D modulations have been shown to be useful for beam shaping [18] as well as for general frequency control [19].

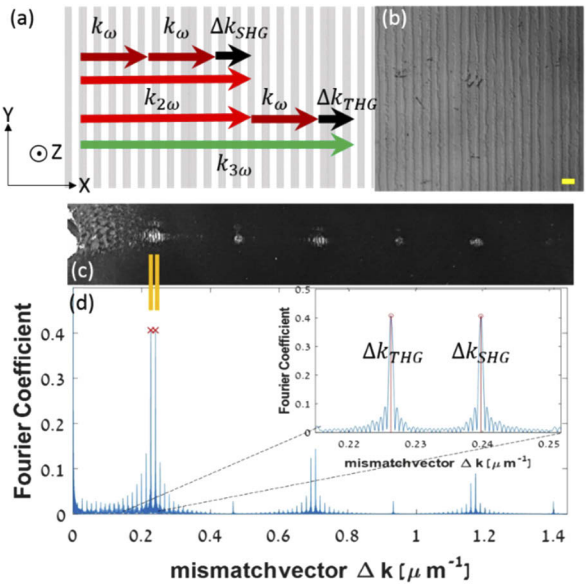

Fig. 1. (a) A schematic picture of the cascaded processes; (x,y,z) refers to the dielectric frame ; $k_{\omega,2\omega,3\omega}$ stands for the wave vectors and $\Delta k_{SHG,THG}$ for the phase-mismatches, with no metric matching between the vector sizes and the pattern in the background. (b) Microscopy picture of the QPPKTP crystal exhibiting the poling pattern; the yellow scale bar is 28 µm long. (c) Far field diffraction pattern from the crystal. In orange are the peaks that correspond to the peaks used for the design. (d) Fourier Transform of the nonlinear modulation pattern, exhibiting two peaks at the mismatch frequencies, *i.e.* $\Delta k_{SHG} = 0.24441 \mu m^{-1}$ for the SHG and $\Delta k_{THG} = 0.22031 \mu m^{-1}$ for the THG.

OSA CONTINUUM

One interesting way of designing nonlinear crystals is by imposing a quasi-periodic structure [20,21], where multiple periods are combined in the same crystal. This enables to phase-match multiple processes simultaneously through different Fourier components of the crystal modulation. These crystals are designed to have a few discrete peaks in their Fourier spectrum, each corresponding to the phase-matching requirements of each process. This concept was originally based on a Fibonacci tiling of the crystal [9,22], although only specific wave-vectors, whose ratio depends on the Fibonacci golden ratio, are available for phase matching in this type of system. The theory was later extended to provide an arbitrary set of wave vectors with the use of the De Brujin's dual-grid method [20,23], which enables to phase-match an arbitrary combination of multiple nonlinear processes, in one dimension [20,21] as well as two dimensions [24].

In order to simultaneously phase-match SHG and THG, we used a quasiperiodic modulation in a KTP crystal. We chose the third-harmonic to be $\lambda_{3\omega} = 527\ nm$, so that the lower harmonics are $\lambda_{2\omega} = 790.5\ nm$, and $\lambda_{\omega} = 1581\ nm$. We considered the following cascading processes: type 0 SHG (all fields are z-polarized) $1581_{(z)} + 1581_{(z)} \rightarrow 790.5_{(z)}$ followed by type II THG (input signal is (z) polarized and the rest are (y) polarized) $790.5_{(z)} + 1581_{(y)} \rightarrow 527_{(y)}$ where y and z stand for the direction of polarization of the waves propagating along the x-axis, (x, y, z) being the crystalline axes. We then calculated the corresponding phase-mismatch values, *i.e.*: $\Delta k_{SHG} = k_{2\omega} - 2k_{\omega}$ and $\Delta k_{THG} = k_{3\omega} - k_{2\omega} - k_{\omega}$, where $k_i = 2\pi n(\lambda_i)/\lambda_i$ is the wave vector. Using the refractive indices of KTP as a function of temperature [25,26] at 100°C, we obtained $\Delta k_{SHG} = 0.24441 \mu m^{-1}$ and $\Delta k_{THG} = 0.22031 \mu m^{-1}$. The flexibility of our design method [20,21] allows us to tailor the nonlinear response of the crystal so that it will provide phase-matching at these two spatial frequencies, with the tiling vectors $\pi/\Delta k_{SHG} = 14.1836 \mu m$ and $\pi/\Delta k_{THG} = 12.7849 \mu m$, respectively. We fabricated a 1-cm-long QPPKTP crystal, where the width of the poled zone is 1 mm. A microscopy image of the selectively etched surface of the fabricated crystal and the associated Fourier spectrum are shown in Fig. 1.

3. Phase-matching conditions

We experimentally determined the phase-matching wavelengths and the corresponding temperatures of the SHG and THG steps in the 1-cm-long QPPKTP sample described in the previous section. The fundamental beam at λ_{ω}, that is used for pumping the QPPKTP crystal, was emitted by a tunable TOPAS optical parametric generator (OPG) with a repetition rate of 10 Hz, a pulse duration of $\tau_{\omega} = 15 ps$ (Full-width at $1/e^2$), and a wavelength tunability with an accuracy of ± 1 nm. The QPPKTP was placed in an oven whose temperature can be tuned from room temperature to 140°C with an accuracy of ± 0.5°C. The longitudinal thermal gradient between the center of the crystal and the entrance or exit face is equal to 0.7°C, while the transverse gradient was estimated to be 0.3 °C. The temperature of the QPPKTP crystal can be assumed to be nearly homogeneous since such a gradient may affect the fifth decimal place of the refractive indices, which cannot modify the phase-matching conditions. The fundamental pump beam is focused inside the crystal with a focal lens $f = 50$ cm; its waist *radius* measured at the center of the crystal is then equal to $w_{\omega} = 205 \pm 21\ \mu m$ (Full-width at $1/e^2$), which leads to a Rayleigh length of ~15 cm, much longer than the crystal length, ensuring propagation in the parallel beam limit. The experiment design enabled to independently measure the energy of the second-harmonic (SH) and third-harmonic (TH) waves. The two corresponding beams were separated using a high reflectivity mirror at 800 nm: the energy at $\lambda_{2\omega}$ was measured by a J3S10 Molectron joulemeter (MJ) placed behind a notch filter at 532-nm, and the energy at $\lambda_{3\omega}$ using also a J3S10 MJ behind a prism. The energy of the incident beam at λ_{ω} was measured before the QPPKTP crystal using a J305 MJ behind a flip mirror. A half-waveplate installed in the input beam path before the QPPKTP allowed us to adjust the polarization of the beam at λ_{ω} according to the required phase-matching condition, *i.e.* that of a pure SHG or that of THG.

OSA CONTINUUM

By tuning the OPG wavelength λ_ω and the QPPKTP temperature T, we identified several situations for which SHG and THG were phase-matched simultaneously, as shown in Fig. 2(a). In this example, the temperature of the QPPKTP crystal was fixed at T = 90.7 °C, and the 2ω and 3ω peaks are centered at λ_ω = 1587 nm and λ_ω = 1586 nm, respectively. The shift between these two wavelengths was within the measurement accuracy, *i.e.* ± 1 nm.

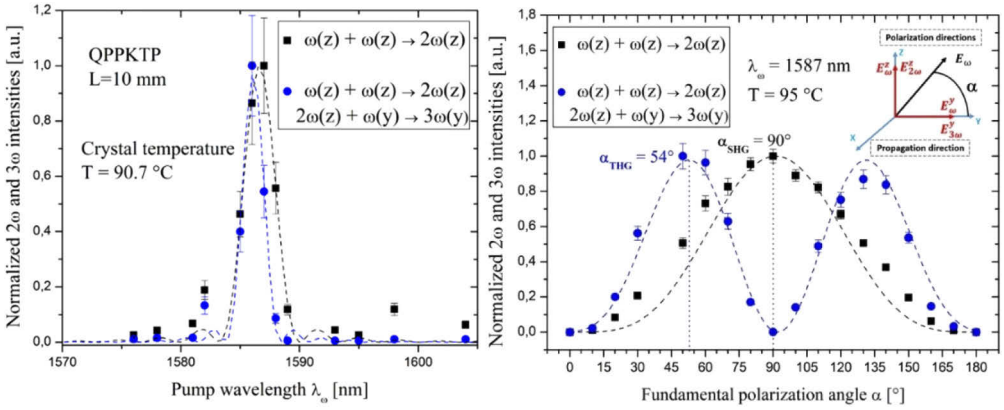

(a) (b)

Fig. 2. (a) Normalized intensities of the second-harmonic (SH) wave and third-harmonic (TH) waves as a function of the QPPKTP temperature when the waves propagate along the *x*-axis, the quantities *(y)* and *(z)* referring to the polarization directions of the interacting waves; the dots correspond to experimental data and the dashed lines to fits. (b) Normalized intensities of the SH and TH waves as a function of the polarization angle α defined in the right inset. The fundamental intensity was lower than 0.5 GW.cm^{-2}, hence pump depletion is negligible here.

Figure 2(a) shows that a concomitant phase-matching exists in the QPPKTP crystal on the one hand, and that the corresponding values of the phase-matching parameters are close to the theoretical ones, *i.e.* λ_ω = 1581 nm and T = 100°C, on the other hand. This agreement between calculations and experiments validates the design of the quasi-periodic grating as well as of the values of the refractive indices as a function of wavelength and temperature.

There is also a satisfying agreement at the level of the wavelength acceptance, $\delta\lambda_\omega$, that is defined as the full width of the phase-matching peak at 0.405 of its maximum. The experimentally measured bandwidths of $\delta\lambda^{SHG}_{\omega\ exp}$ = 3.4 *nm* and $\delta\lambda^{THG}_{\omega\ exp}$ = 2.3 *nm*, according to Fig. 2(a), are slightly wider than the theoretical values, i.e. $\delta\lambda^{SHG}_{\omega calc}$ = 2.2 *nm* and $\delta\lambda^{THG}_{\omega calc}$ = 1.8 *nm*. This weak discrepancy is probably mainly due to some small imperfections in fabrication. Since the product of the interacting length by the acceptance is constant, we conclude that the effective interaction length for the SHG and THG, L^{SHG}_{eff} and L^{THG}_{eff} respectively, are slightly smaller than the geometrical length = 1*cm*, *i.e.* $L^{SHG}_{eff} = L(\delta\lambda^{SHG}_{\omega calc}/\delta\lambda^{SHG}_{\omega\,\mathrm{exp}}) = 6.6mm$ and $L^{THG}_{eff} = L(\delta\lambda^{THG}_{\omega calc}/\delta\lambda^{THG}_{\omega\,\mathrm{exp}}) = 7.8mm$.

A final optimization led to a maximal THG conversion efficiency reached for λ_ω = 1587 nm and T = 95°C. The corresponding polarization curves are shown in Fig. 2(b) where α is the angle between the polarization of the fundamental wave and the *y*-axis of the QPPKTP crystal. There is a perfect agreement between calculation and measurement, the optimal angle for a Type 0 SHG being found at $\alpha = 90°$, while it is $\alpha = 54°$ for THG. Note that these two values of angle can be easily calculated in the undepleted pump approximation (UPA) because the SH intensity is simply proportional to the square of the fundamental intensity, which gives $I_{2\omega} \propto \sin^4(\alpha)$, and

OSA CONTINUUM

the cascaded TH intensity depends on the product of the fundamental and SH intensities, *i.e.* $I_{3\omega} \propto \sin^4(\alpha)\cos^2(\alpha)$. These values of optimal polarization angles obviously remain the same in the depleted pump regime.

These latter experimental conditions of temperature, wavelength and polarization were kept for measuring the SHG and THG conversion efficiencies, as described in the next section.

4. Conversion efficiencies

The conversion efficiencies, expressed as the power ratios $\eta_{SHG} = \varepsilon_{2\omega}(L)/\varepsilon_{2\omega}(0)$ and $\eta_{THG} = \varepsilon_{3\omega}(L)/\varepsilon_{\omega}(0)$, were measured using the experimental setup described in the previous section. First, we considered SHG alone, so the polarization angle α was fixed at $90°$. Second, we performed THG, which can be achieved for α=$54°$. In this situation, while η_{SHG} decreased to the value of 17% as shown in Fig. 3(a), whereas THG was optimized, the conversion efficiency η_{THG} reaching a maximal value of 40% from a fundamental intensity of about 1.5 GW/cm^2 that corresponds to a fundamental energy of 20µJ. The normalized conversion efficiency with respect to the peak power defined as $([P_{3\omega}(L)/P_{\omega}(0)]L)^2$ is 43.1% /MW.cm^2. Figure 3(a) shows that the SH wave was depleted when the THG was optimized since the corresponding SHG energy conversion efficiency dropped from 45%, to 17%.

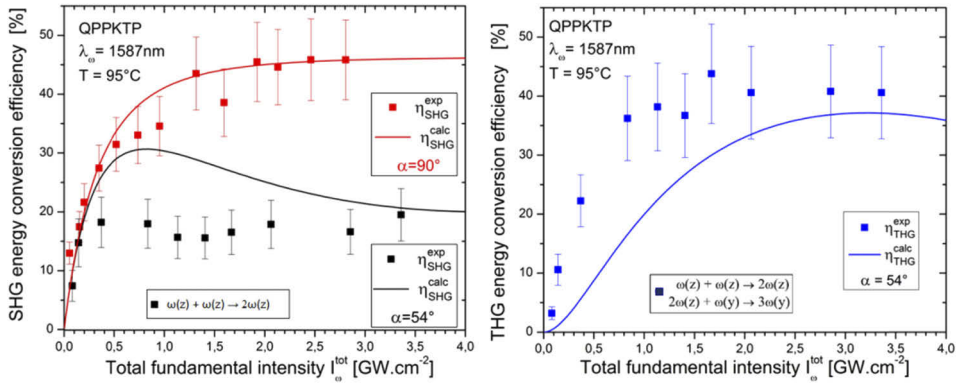

(a) **(b)**

Fig. 3. SHG (a) and THG (b) energy conversion efficiencies as a function of the total incident fundamental intensity. The dots correspond to experimental data and the continuous lines stand for the interpolations.

The comparison with theory was performed using a numerical calculation of the following coupled system of equations relative to real amplitudes, *i.e.* the *moduli* of the complex amplitudes of the electric fields of the interacting waves written $|E_{\omega,2\omega,3\omega}|$. It is assumed that SHG and THG are quasi-phase-matched along the x-axis of the QPPKTP crystal. Therefore, we consider only a single Fourier component for each one of these two processes, so that the effective nonlinear coefficient is given by the product of the material's second-order susceptibility $\chi^{(2)}$ with the corresponding Fourier coefficient F. This system of equations can be written as:

$$\begin{cases} \frac{\partial|E^z_{\omega}(X)|}{\partial X} = -\frac{\pi}{\lambda_{\omega} n_z(\lambda_{\omega})}\chi^{(2)}_{33}(\omega = 2\omega - \omega)F^{SHG}|E^z_{2\omega}(X)|.|E^{z\,*}_{\omega}(X)| \\ \frac{\partial|E^y_{\omega}(X)|}{\partial X} = -\frac{\pi}{\lambda_{\omega} n_y(\lambda_{\omega})}\chi^{(2)}_{24}(\omega = 3\omega - 2\omega)F^{THG}|E^y_{3\omega}(X)|.|E^{z*}_{2\omega}(X)| \\ \frac{\partial|E^z_{2\omega}(X)|}{\partial X} = +\frac{\pi}{\lambda_{2\omega} n_z(\lambda_{2\omega})}\chi^{(2)}_{33}(2\omega = \omega + \omega)F^{SHG}|E^z_{\omega}(X)|.|E^z_{\omega}(X)| \\ \quad -\frac{\pi}{\lambda_{2\omega} n_z(\lambda_{2\omega})}\chi^{(2)}_{24}(2\omega = 3\omega - \omega)F^{THG}|E^y_{3\omega}(X)|.|E^{y*}_{\omega}(X)| \\ \frac{\partial|E^y_{3\omega}(X)|}{\partial X} = +\frac{\pi}{\lambda_{3\omega} n_y(\lambda_{3\omega})}\chi^{(2)}_{24}(3\omega = \omega + 2\omega)F^{THG}|E^y_{\omega}(X)|.|E^z_{2\omega}(X)| \end{cases} . \quad (1)$$

OSA CONTINUUM

Here the quantity X is the longitudinal coordinate along the x-axis, the superscripts y and z stand for the directions of the electric fields, and the wavelengths are the optimal ones derived experimentally, *i.e.* $\lambda_\omega = 1587.0nm$, $\lambda_{2\omega} = 793.5nm$ and $\lambda_{3\omega} = 529.0nm$. The values of the principal refractive indices $n_y(\lambda_{\omega/3\omega})$ and $n_z(\lambda_{\omega/2\omega})$ are given in Table 1; they are calculated according to the considered wavelengths at the working temperature from the dispersion equations of Refs. [25,26]. The second-order nonlinear coefficients $\chi^{(2)}_{24}$ and $\chi^{(2)}_{33}$, also given in Table 1, are calculated from the data at room temperature of Ref. [27] using Miller rule. The Fourier amplitudes F_{SHG} and F_{THG} can be calculated using the method outlined in Ref. [20], but here they are adjustment parameters for fitting the experimental data. Since there is no analytical solution to Eq. (1), the comparison with theory was performed using a parametric numerical resolution based on the *Runge-Kutta* method.

Table 1. Wavelengths λ_{ω_i} where ω_i stands for the frequencies ω, 2ω or 3ω, pulse durations τ_{ω_i}, principal refractive indices $n_y(\lambda_{\omega/3\omega})$ and $n_y(\lambda_{\omega/3\omega})$ [26], beam wait *radii* w_{ω_i}, Fresnel transmissions $T^{y,z}_{\omega_i}$ and nonlinear coefficients $\chi^{(2)}_{ij}$ used for the numerical integration of Eqs. (1) [27].

	λ_{ω_i} [nm]	τ_{ω_i} [ps]	$n_y(\lambda_{\omega_i})$	$n_z(\lambda_{\omega_i})$	w_{ω_i} [μm]	$T^z_{\omega_i}$	$T^y_{\omega_i}$	$\chi^{(2)}_{33}$ [pmV^{-1}]	$\chi^{(2)}_{24}$ [pmV^{-1}]
ω	1587	15.0	1.7363	1.8150	205	0.917	0.929	16.1	3.8
2ω	793.5	10.6	-	1.8445	145	0.912	-	19.2	4.8
3ω	529	8.7	1.7907	-	118	-	0.920	-	5.3

The study of the wavelength acceptances described in the previous section shows that the effective interaction length is slightly smaller than the geometrical length of the QPPKTP crystal, and that this effective length is not the same for SHG and THG. Then the numerical integration of Eq. (1) was made from $X = 0$, *i.e.* the entrance of the crystal, and $X = l_{eff}^{SHG} = 6.6\ mm$ for SHG, to $X = l_{eff}^{THG} = 7.8mm$ for THG.

The electric fields in Eq. (1) are the internal fields inside the QPPKTP crystal. The values of the *moduli* of the complex amplitudes of the fundamental electric fields at the entrance of the crystal, i.e. $|E^y_\omega(X=0)|$ and $|E^z_\omega(X=0)|$ that have to be taken for the integration of Eq. (1) are linked to the total experimental energy of the incident fundamental beam $\varepsilon^{tot}_\omega(X=0)$ by the following equations (assuming plane waves with temporal and transverse Gaussian profiles):

$$\begin{cases} |E^y_\omega(X=0)| = \sqrt{\frac{\mu_0 c}{n_y(\lambda_\omega)\kappa_\omega} T^y_\omega \cos^2(\alpha) \varepsilon^{tot}_\omega(X=0)} \\ |E^z_\omega(X=0)| = \sqrt{\frac{\mu_0 c}{n_z(\lambda_\omega)\kappa_\omega} T^z_\omega \sin^2(\alpha) \varepsilon^{tot}_\omega(X=0)} \end{cases} \tag{2}$$

with

$$\begin{cases} T^{y,z}_\omega = \frac{4 n_{y,z}(\lambda_\omega)}{[1+n_{y,z}(\lambda_\omega)]^2} \\ \kappa_\omega = \left(\frac{\pi}{2}\right)^{3/2} \frac{\tau_\omega}{2} w^2_\omega \end{cases} . \tag{3}$$

The quantities $T^{y,z}_\omega$ correspond to the Fresnel transmission in normal incidence, the light being polarized along the y-axis or z-axis respectively, and α=90° for the SHG alone and α=54° for the optimized THG. The quantity τ_ω corresponds to the pulse duration and w_ω to the beam *radii*.

In the same way, the calculated energy of the generated SH and TH waves at the exit of the QPPKTP crystal, *i.e.* $\varepsilon_{2\omega}(X=L)$ and $\varepsilon_{3\omega}(X=L)$, are linked to the *moduli* of the calculated SH and TH complex amplitudes, *i.e.* $|E^z_{2\omega}(X=L)|$ and $|E^y_{3\omega}(X=L)|$, by:

$$\begin{cases} \varepsilon_{2\omega}(X=L) = \kappa_{2\omega} T^z_{2\omega} \frac{n_z(\lambda_{2\omega})}{\mu_0 c} |E^z_{2\omega}(X=L)|^2 \\ \varepsilon_{3\omega}(X=L) = \kappa_{3\omega} T^y_{3\omega} \frac{n_y(\lambda_{3\omega})}{\mu_0 c} |E^y_{3\omega}(X=L)|^2 \end{cases} \tag{4}$$

OSA CONTINUUM

with

$$\begin{cases} T_{2\omega}^{z} = \frac{4n_z(\lambda_{2\omega})}{[1+n_z(\lambda_{2\omega})]^2} \\ \kappa_{2\omega} = \left(\frac{\pi}{2}\right)^{3/2} \frac{\tau_{2\omega}}{2} w_{2\omega}^2 \\ T_{3\omega}^{y} = \frac{4n_y(\lambda_{3\omega})}{[1+n_y(\lambda_{3\omega})]^2} \\ \kappa_{3\omega} = \left(\frac{\pi}{2}\right)^{3/2} \frac{\tau_{3\omega}}{2} w_{3\omega}^2 \end{cases} \tag{5}$$

where the Gaussian relations apply regarding the pulse durations τ_ω, $\tau_{2\omega}$ and $\tau_{3\omega}$ as well as the beam *radii* w_ω, $w_{2\omega}$ and $w_{3\omega}$, *i.e.*:

$$\begin{cases} w_{2\omega} = \frac{w_\omega}{\sqrt{2}}, \tau_{2\omega} = \frac{\tau_\omega}{\sqrt{2}} \\ w_{3\omega} = \frac{w_\omega}{\sqrt{3}}, \tau_{3\omega} = \frac{\tau_\omega}{\sqrt{3}} \end{cases} . \tag{6}$$

The numerical values of the Fresnel transmissions, beam waist *radii* and pulse durations are given in Table 1.

The system of Eq. (1) was first solved for the SHG case only by taking α=*90°*. We performed a parameter adjustment on the Fourier coefficient F_{SHG}. The best fit was found for F_{SHG} = 0.28, which is 30% lower than the theoretical value. The shape of the fitting curve is in excellent agreement with the experimental data as shown by the red curve of Fig. 3(a). Afterwards, this value of F_{SHG} was taken for the second step of integration where the whole system has been considered, *i.e.* for α=*54°*. The Fourier coefficient F_{THG} was then taken also as a fitting parameter and ended up only 8% smaller than its theoretical value, *i.e.* F_{THG} = 0.368. These deviations from the theoretical Fourier coefficient are thought to be due to fabrication defaults. But the agreement remains very good between the theoretical and experimental curves as shown by the black curves of Fig. 3(a) and by Fig. 3(b). Note that the high values of the conversion efficiency for both SHG and THG are well corroborated by the behaviors of the curves of Fig. 3, which undoubtedly indicate that SHG as well as THG are achieved in the depleted pump regime.

5. Conclusion

We demonstrated a 40% THG energy conversion efficiency in a quasi-periodically poled KTP crystal pumped with an energy as low as 20 μJ. This is the highest THG efficiency ever reported to the best of our knowledge. Previous records using also a quasi-periodic poling structure were 23% [9], and 30.7% in a single KDP crystal allowing simultaneous birefringent phase-matching [12]. Note that using $\chi^{(3)}$ interactions for THG results in efficiencies of single percent only [8].

Our work opens the way to exciting developments regarding frequency up-conversion for numerous applications, in particular for the generation in the ultra-violet range around 330 nm starting from a laser around 1 μm. Moreover, it opens new possibilities in quantum optics for TPG by a $\chi^{(2)}$ cascaded spontaneous parametric down conversion [17] of a 527 nm pump for generating a three-photon state at 1581 nm in a compact single nonlinear crystal, which is an alternative of using a $\chi^{(3)}$ process in a birefringent crystal [28]. Intracavity quasi-phase-matching may also be interesting in this context [29].

Funding

Israel Science Foundation (1415/17); ANR/FNS PRCI France-Switzerland (16707).

Acknowledgments

All the authors wish to thank Imaginano (the France Israël Associated International Laboratory with CNRS – Weizmann Institute of Science - Tel Aviv University – Hebrew University of Jerusalem).

OSA CONTINUUM

Disclosures

The authors declare no conflicts of interest.

References

1. P. Franken, A. E. Hills, C. W. Peters, and G. Weinreich, "Generation of Optical Harmonics," Phys. Rev. Lett. **7**(4), 118–119 (1961).
2. J. A. Giordmaine and R. C. Miller, "Tunable coherent parametric oscillation in $LiNbO_3$ at optical frequencies," Phys. Rev. Lett. **14**(24), 973–976 (1965).
3. Y. X. Fan, R. C. Eckardt, R. L. Byer, J. Nolting, and R. Wallenstein, "Visible BaB2O4 optical parametric oscillator pumped at 355 nm by a singleaxialmode pulsed source," Appl. Phys. Lett. **53**(21), 2014–2016 (1988).
4. A. V. Simakin and G. A. Shafeev, "Initiation of nuclear reactions under laser irradiation of Au nanoparticles in the aqueous solution of Uranium salt," Appl. Phys. A **101**(1), 199–203 (2010).
5. R. P. Schmid, T. Schneider, and J. Reif, "Optical processing on a femtosecond time scale," Opt. Commun. **207**(1-6), 155–160 (2002).
6. V. G. Dmitriev and R. Singh, "Generation of polarization squeezed light in PPNC," Int. J. Quantum Inform. **01**(3), 403–416 (2003).
7. A. V Belinsky and R. Singh, "Simultaneous nonlinear conversion of light in periodically poled crystals," Quantum Electron. **48**(7), 611–614 (2018).
8. F. Gravier and B. Boulanger, "Third order frequency generation in TiO_2 rutile and $KTiOPO_4$," Opt. Mater. **30**(1), 33–36 (2007).
9. S. N. Zhu, Y. Y. Zhu, and N. Ben Ming, "Quasi–Phase-Matched Third-Harmonic Generation in a Quasi-Periodic Optical Superlattice," Science **278**(5339), 843–846 (1997).
10. H. Qi, Z. Wang, F. Yu, X. Sun, X. Xu, and X. Zhao, "Cascaded third-harmonic generation with one KDP crystal," Opt. Lett. **41**(24), 5823–5826 (2016).
11. M. Marangoni, M. Lobino, and R. Ramponi, "Simultaneously phase-matched second- and third-harmonic generation from 1.55 μm radiation in annealed proton-exchanged periodically poled lithium niobate waveguides," Opt. Lett. **31**(18), 2707–2709 (2006).
12. B. Boulanger, J. P. Fève, P. Delarue, I. Rousseau, and G. Marnier, "Cubic optical nonlinearity of $KTiOPO_4$," J. Phys. B: At., Mol. Opt. Phys. **32**(2), 475–488 (1999).
13. V. Boutou, A. Vernay, C. Félix, F. Bassignot, M. Chauvet, D. Lupinski, and B. Boulanger, "Phase-matched second-harmonic generation in a flux grown KTP crystal ridge optical waveguide," Opt. Lett. **43**(15), 3770–3773 (2018).
14. P. S. Banks, M. D. Feit, and M. D. Perry, "High-intensity third-harmonic generation," J. Opt. Soc. Am. B **19**(1), 102 (2002).
15. K. Fradkin-Kashi, A. Arie, P Urenski, and G. Rosenman, "Multiple Nonlinear Optical Interactions with Arbitrary Wave Vector Differences," Phys. Rev. Lett. **88**(2), 023903 (2001).
16. A. Bahabad, R. Lifshitz, N. Voloch, and A. Arie, "Nonlinear photonic quasicrystals for novel optical devices," Philos. Mag. **88**(13-15), 2285–2293 (2008).
17. H. Hübel, D. R. Hamel, A. Fedrizzi, S. Ramelow, K. J. Resch, and T. Jennewein, "Direct generation of photon triplets using cascaded photon-pair sources," Nature **466**(7306), 601–603 (2010).
18. S. Trajtenberg-Mills and A. Arie, "Shaping light beams in nonlinear processes using structured light and patterned crystals," Opt. Mater. Express **7**(8), 2928–2942 (2017).
19. A. Leshem, R. Shiloh, and A. Arie, "Experimental realization of spectral shaping using nonlinear optical holograms," Opt. Lett. **39**(18), 5370–5373 (2014).
20. R. Lifshitz, A. Arie, and A. Bahabad, "Photonic Quasicrystals for Nonlinear Optical Frequency Conversion," Phys. Rev. Lett. **95**(13), 133901 (2005).
21. A. Bahabad, N. Voloch, A. Arie, and R. Lifshitz, "Experimental confirmation of the general solution to the multiple-phase-matching problem," J. Opt. Soc. Am. B **24**(8), 1916 (2007).
22. Z. V. Vardeny, A. Nahata, and A. Agrawal, "Optics of photonic quasicrystals," Nat. Photonics **7**(3), 177–187 (2013).
23. N. G. De Brujin, "Algebraic theory of Penrose's non-periodic tilings of the plane," Indag. Math. (Proc.) **84**(1), 39–52 (1981).
24. A. Bahabad, A. Ganany-Padowicz, and A. Arie, "Engineering two-dimensional nonlinear photonic quasi-crystals," Opt. Lett. **33**(12), 1386–1388 (2008).
25. S. Emanueli and A. Arie, "Temperature-dependent dispersion equations for $KTiOPO_4$ and $KTiOAsO_4$," Appl. Opt. **42**(33), 6661–6665 (2003).
26. K. Kato, "Parametric Oscillation at 3.2 μm in KTP Pumped at 1.064 μm," IEEE J. Quantum Electron. **27**(5), 1137–1140 (1991).
27. B. Boulanger, J. P. Fève, G. Marnier, B. Ménaert, X. Cabirol, P. Villeval, and C. Bonnin, "Relative sign and absolute magnitude of $d^{(2)}$ nonlinear coefficients of KTP from second-harmonic-generation measurements," J. Opt. Soc. Am. B **11**(5), 750–757 (1994).
28. J. Douady and B. Boulanger, "Experimental demonstration of a pure third-order optical parametric downconversion process," Opt. Lett. **29**(23), 2794–2796 (2004).

OSA CONTINUUM

29. N. V. Kravtsov, G. D. Laptev, I. I. Naumova, A. A. Novikov, V. V. Firsov, and A. S. Chirkin, "Intracavity quasi-phase matched frequency summing in a laser based on a periodically poled active nonlinear Nd:Mg:$LiNbO_3$crystal," Quantum Electron. **32**(10), 923–924 (2002).